

Energy Gaps in Graphene Nanoribbons

Young-Woo Son,^{1,2} Marvin L. Cohen,^{1,2} and Steven G. Louie^{1,2,}¹Department of Physics, University of California at Berkeley, Berkeley, CA 94720²Materials Sciences Division, Lawrence Berkeley National Laboratory, Berkeley, CA 94720

(Dated: March 23, 2024)

Based on a first-principles approach, we present scaling rules for the band gaps of graphene nanoribbons (GNRs) as a function of their widths. The GNRs considered have either arm chair or zigzag shaped edges on both sides with hydrogen passivation. Both varieties of ribbons are shown to have band gaps. This differs from the results of simple tight-binding calculations or solutions of the Dirac's equation based on them. Our ab initio calculations show that the origin of energy gaps for GNRs with arm chair shaped edges arises from both quantum confinement and the crucial effect of the edges. For GNRs with zigzag shaped edges, gaps appear because of a staggered sublattice potential on the hexagonal lattice due to edge magnetization. The rich gap structure for ribbons with arm chair shaped edges is further obtained analytically including edge effects. These results reproduce our ab initio calculation results very well.

PACS numbers: 73.22.-f, 75.70.Ak, 72.80.Rj

The electronic structure of nanoscale carbon materials such as fullerenes and carbon nanotubes has been the subject of intensive research during the past two decades [1] because of fundamental scientific interest in nanomaterials and because of their versatile electronic properties that are expected to be important for future nanoelectronics [2, 3]. Among the carbon nanostructures, a simple variation of graphene, ribbons with nanometer sized widths, has been studied extensively [4, 5, 6, 7, 8, 9, 10, 11, 12, 13, 14, 15]. Because of recent progress in preparing single graphite layers on conventional device setups, the graphene nanoribbons (GNRs) with varying widths can be realized either by cutting [16] mechanically exfoliated graphenes [17, 18] or by patterning epitaxially grown graphenes [19, 20].

Since GNRs are just geometrically terminated single graphite layers, their electronic structures have been modeled by imposing appropriate boundary conditions on Schrodinger's equation with simple tight-binding (TB) approximations based on s -states of carbon [4, 5, 6, 7] or on a 2-dimensional free massless particle Dirac's equation with an effective speed of light ($\sim 10^6$ m/s) [8, 9, 10]. Within these models, it is predicted that GNRs with arm chair shaped edges can be either metallic or semiconducting depending on their widths [4, 5, 6, 7, 8, 9, 10], and that GNRs with zigzag shaped edges are metallic with peculiar edge states on both sides of the ribbon regardless of its widths [4, 5, 6, 7, 8, 9, 10, 11, 12, 13, 14].

Although the aforementioned models are known to describe the low energy properties of graphene very well [17, 18, 19, 20, 21, 22], a careful consideration of edge effects in nanometer sized ribbons are required to determine their bandgaps because, unlike the situation in graphene, the bonding characteristics between atoms change abruptly at the edges [7, 15]. Moreover, the spin degree of freedom is also important because the GNRs with zigzag shaped edges have narrow band edge states

at the Fermi energy (E_F) implying possible magnetization at the edges [4, 11, 12, 13]. Motivated by the recent experimental progress in this area, we have carried out first-principles calculation and theoretical analysis to explore the relation between the bandgap and the geometries of GNRs.

In this Letter, we show that GNRs with hydrogen passivated arm chair or zigzag shaped edges both always have nonzero and direct bandgaps. The origins of the bandgaps for the different types of homogeneous edges vary. The bandgaps of GNRs with arm chair shaped edges originate from quantum confinement, and edge effects play a crucial role. For GNRs with zigzag shaped edges, the bandgaps arise from a staggered sublattice potential due to spin ordered states at the edges [4, 11, 12, 13]. Although the ribbon widths and energy bandgaps of the GNRs are related to each other primarily in inverse proportion, there is a rich structure in the ratio of the proportionalities as in the behavior of carbon nanotubes [1]. For GNRs with arm chair edges, analytic scaling rules for the size of the bandgaps are obtained as a function of width including the effect of the edges and give a good agreement with our first-principles calculations.

Our electronic structure calculation employs the first-principles self-consistent pseudopotential method [23] using the local (spin) density approximation (L(S)DA) [23, 24]. An energy cutoff (for a real space mesh size) of 400 Rydbergs is employed and a double- η plus polarization basis set [23] is used for the localized basis orbitals to deal with the many atoms in a unit cell of the GNRs of various widths. We obtained the electron density by integrating the density matrix with a Fermi-Dirac distribution [23, 25]. The geometry for each GNR studied is fully relaxed until the force on each of the atoms is less than 16 pN. A k -point sampling of 32 (96) k -points that are uniformly positioned along the 1D Brillouin zone is employed for GNRs with arm chair (zigzag) shaped edges.

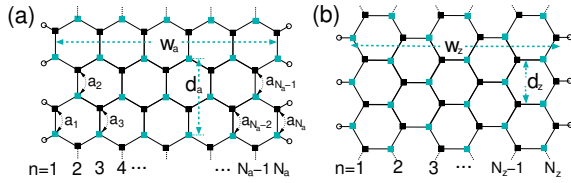


FIG. 1: (a) Schematic of a 11-AGNR. The empty circles denote hydrogen atoms passivating the edge carbon atoms, and the black and grey rectangles represent atomic sites belonging to different sublattices in the graphene structure. The 1D unit cell distance and ribbon width are represented by d_a and w_a respectively. The carbon-carbon distances on the n -th dimer line is denoted by a_n . (b) Schematic of a 6-ZGNR. The empty circles and rectangles follow the same convention described in (a). The 1D unit cell distance and the ribbon width are denoted by d_z and w_z respectively.

We have tested the change of gap size by increasing the vacuum between edges from 20 to 40 Å and between planes from 16 to 25 Å and found no changes.

Following previous convention [4, 5, 6, 7, 8, 9, 10, 11, 12, 13, 14, 15], the GNRs with arm chair shaped edges on both sides are classified by the number of dimer lines (N_a) across the ribbon width as shown in Fig. 1 (a). Likewise, ribbons with zigzag shaped edges on both sides are classified by the number of the zigzag chains (N_z) across the ribbon width [Fig. 1 (b)]. We refer to a GNR with N_a dimer lines as a N_a -AGNR and a GNR with N_z zigzag chains as a N_z -ZGNR.

Our calculations show that the N_a -AGNRs are semiconductors with energy gaps which decrease as a function of increasing ribbon widths (w_a). The variations in energy gap however exhibit three distinct family behaviors [Fig. 2]. Moreover, the energy gaps obtained by a simple TB model are quite different from those by first-principles calculations. The TB results using a constant nearest neighbor hopping integral, $t = 2.7$ eV [22] between π -electrons are summarized as function of width in Fig. 2 (a). It shows that a N_a -AGNR is metallic if $N_a = 3p + 2$ (where p is a positive integer) or otherwise, it is semiconducting, in agreement with previous calculations [4, 5, 6, 7, 8, 9, 10]. The gap of a N_a -AGNR (Δ_a) is inversely proportional to its width, separated into basically two groups with a hierarchy of gap size given by $\Delta_{3p} & \Delta_{3p+1} > \Delta_{3p+2} (= 0)$ for all p 's. For the first-principles calculations, however, there are no metallic nanoribbons. The gaps as a function of ribbon width are now well separated into three different categories (or family structures) as shown in Fig. 2 (b). Moreover, the gap size hierarchy is also changed to $\Delta_{3p+1} > \Delta_{3p} > \Delta_{3p+2} (\neq 0)$. For example, in the first-principles calculation for $p = 13$, the lowest energy gap is $\Delta_{38} = 45$ meV and $\Delta_{40} = 39$ meV, all of which are quite larger values compared to those (0 and 2 meV respectively) obtained from TB approximations. The first-principles band structures of N_a -AGNRs are shown in Fig. 2 (c) for $N_a = 12, 13$, and 14. They

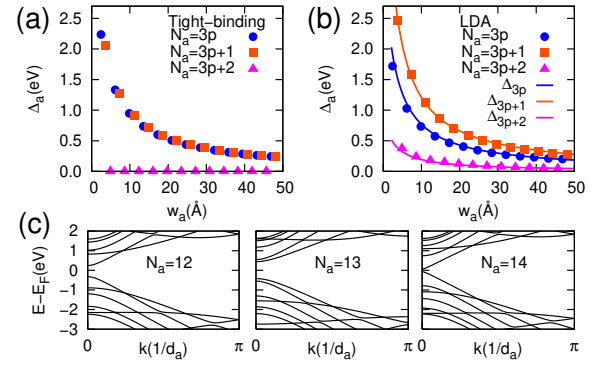


FIG. 2: (color online) The variation of bandgaps of N_a -AGNRs as a function of width (w_a) obtained (a) from TB calculations with $t = 2.70$ (eV) and (b) from first-principles calculations (symbols). The solid lines in (b) are from Eq. (1). (c) First-principles band structures of N_a -AGNRs with $N_a = 12, 13$, and 14, respectively.

exhibit direct bandgaps at $kd_a = 0$ for all cases.

A determining factor in the semiconducting behavior of N_a -AGNR is quantum confinement which can be characterized by $N_a^{-1} w_a^{-1}$ [4, 5, 6, 7, 8, 9, 10]. In addition, as will be discussed below, the edge effects play a crucial role and force the $(3p + 2)$ -AGNRs (predicted to be metallic by TB model) to be semiconductors. The edge carbon atoms of our AGNRs are passivated by hydrogen atoms (by some foreign atoms/molecules in general) so that the bonds between hydrogen and carbon and the onsite energies of the carbons at the edges would be different from those in the middle of the AGNRs. The bonding distances between carbon atoms at the edges are also expected to change accordingly. Such effects have been observed in large aromatic molecules, e.g., ovalene ($C_{32}H_{14}$) [26]. In Fig. 3 (a), we show that the bond lengths parallel to dimer lines at edges (a_1 and a_{N_a} for N_a -AGNR in Fig. 1 (a)) are shortened by 3.3–3.5% for the 12-, 13-, and 14-AGNR as compared to those in the middle of the ribbon. From the analytic expressions for TB matrix elements between carbon atoms in Ref. 27, a 3.5% decrease in interatomic distance from 1.422 Å would induce a 12% increase in the hopping integral between π -orbitals.

To see the consequence of such effects more clearly, we introduce a lattice model [Fig. 3 (b)] which is equivalent to the AGNRs within the TB approximation [4, 5, 6, 7]. The set of eigenvalues of a brick type lattice shown in Fig 3.(b) at $kd_a = 0$ is further equivalent to that of a two-leg ladder system with N_a rungs [4, 5, 6, 7]. The Hamiltonian of this simpler model can be written as $H = \sum_{n=1}^{N_a} \sum_{m=1}^2 \epsilon_m a_{n,m}^\dagger a_{n,m} + \sum_{n=1}^{N_a} t_{n,n+1}^\dagger (a_{1,n}^\dagger a_{2,n+1} + h.c.)$; where ϵ_m denote a site, ϵ_m site energies, $t_{n,m+1}^\dagger$ and t_n^\dagger the nearest neighbor hopping integrals within each leg and between the legs respectively, and $a_{n,m}$ the annihilation operator of π -electrons on the n -th site of the m -th leg. As

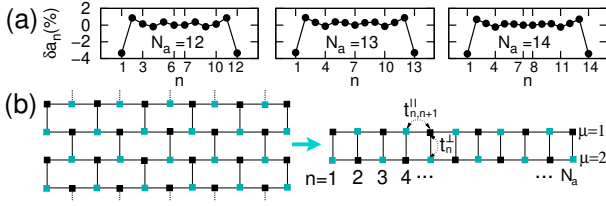


FIG. 3: (a) The ratio of the calculated change in the carbon-carbon distance (δa_n) (see Fig. 1(a)) to the carbon-carbon distance in the middle of the N_a -AGNRs, i.e., $\frac{\delta a_n}{a_c} = \frac{a_n - a_c}{a_c}$ where $a_c = a_6 = a_7 = 1.424$ Å for $N_a = 12$, $a_c = a_7 = 1.422$ Å for $N_a = 13$, and $a_c = a_7 = a_8 = 1.423$ Å for $N_a = 14$, respectively. (b) Topologically equivalent structure to the N_a -AGNR shown in Fig. 1(a). For the special case of $k = 0$, a lattice with periodic ladders (left) can be folded into a two-leg ladder with N_a rungs (right).

discussed above and shown in Fig. 3(a), t_n^2 and μ_m at the edges would differ from those in the middle of GNRs. Hence, considering the simplest but essential variation from the exact solvable model to approximate the realistic situations, we assume that $t_1^2 = t_{N_a}^2 (1 + \epsilon)t$ and $t_n^2 = t$ for $n = 2$; $\mu_{N_a} = \mu_1$, and $t_{n,n+1}^{jj} = t$ for all n 's. The site energies are set at $\mu_m = \mu_0$ for $n = 1$ and N_a and 0 otherwise regardless of ϵ . This model Hamiltonian is solved perturbatively and the resulting energy gaps to the first order in ϵ and μ_0 are as follows,

$$\begin{aligned} \epsilon_{3p} &= \epsilon_{3p}^0 - \frac{8t}{3p+1} \sin^2 \frac{p}{3p+1}; \\ \epsilon_{3p+1} &= \epsilon_{3p+1}^0 + \frac{8t}{3p+2} \sin^2 \frac{(p+1)}{3p+2}; \\ \epsilon_{3p+2} &= \epsilon_{3p+2}^0 + \frac{2j\epsilon}{p+1}; \end{aligned} \quad (1)$$

where ϵ_{3p}^0 , ϵ_{3p+1}^0 and ϵ_{3p+2}^0 are the gaps of the ideally terminated ribbon when $\epsilon = \mu_0 = 0$. They are given by $t \left[4 \cos \frac{p}{3p+1} - 2 \right]$, $t \left[4 \cos \frac{(p+1)}{3p+2} - 2 \right]$ and 0 respectively. The zeroth-order gaps are identical to the values obtained from numerical calculations in Fig. 2(a) [4, 5, 6, 7]. With $t = 2.7$ (eV) [22] and $\epsilon = 0.12$, the calculated gaps obtained using Eq. (1) are in good agreement with our LDA results [Fig. 2(b)]. This implies that the 12% increase of the hopping integrals between carbon atoms at the edges opens the gaps of the $(3p+2)$ -AGNRs and decreases (increases) the gaps of $3p$ -AGNRs ($(3p+1)$ -AGNRs). This analysis provides the physical explanation of the changes in the gap hierarchy discussed before. We note that there is no contribution from the variation in the site energies (μ_0) at the edges to first order.

Next, we find that nanoribbons with zigzag shaped edges also have direct bandgaps which decrease with increasing width (w_z). The eigenstates of the ZGNRs near E_F , without considering spins, have a peculiar edge-state structure. As noted earlier within the tight-binding picture [4], there are two edge states decaying into the cen-

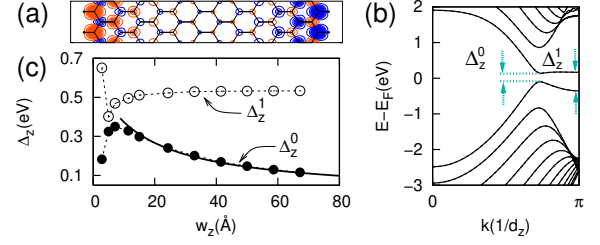


FIG. 4: (color online) (a) Contour graph for the density of states (DOS) of a 12-ZGNR (the density is integrated over the normal direction to the ribbon plane). The lowest (highest) contour of $0.4 \times 10^4 a_0^2$ is drawn by a thick blue (red) line and the spacing for blue (red) lines is $1.0 \times 10^4 a_0^2$ ($a_0 = \text{Bohr radius}$). (b) The band structure of a 12-ZGNR. The $+$ - and $-$ -spin states are degenerate in all energy bands. ϵ_z^0 and ϵ_z^1 denote the direct bandgap and the energy splitting at $kd_z = 0$ and π , respectively. (c) The variation of ϵ_z^0 and ϵ_z^1 as a function of the width (w_z) of N_z -ZGNRs. The solid line is a fit curve for ϵ_z^0 ($N_z = 8$) and the dotted lines are drawn to guide the eyes.

ter of the ZGNR with a decay profile depending on their momentum as $e^{-\kappa x}$ where $\kappa = \frac{2}{3d_z} \ln 2 \cos \frac{kd_z}{2}$ ($\frac{2}{3} = \frac{2}{3} kd_z$, $d_z = \text{unit cell length shown in Fig. 1(b)}$). Our first-principles calculation also predicts a set of doubly degenerate edge-state bands at E_F when not considering spins (not shown here). Since the edge-states around E_F form flat bands, they give rise to a very large density of states at E_F . Thus in nanoscale systems on-site repulsions could make the ZGNRs magnetic [4], unlike the case with two-dimensional graphene which has a zero density of states at E_F . As pointed out in a TB study earlier [4] and later confirmed by first-principles studies [11, 12, 13], our LSDA calculation also shows that the ground state of ZGNRs with hydrogen passivated zigzag edges indeed have finite magnetic moments on each edge with negligible change in atomic structure [11, 12, 13, 14].

Upon inclusion of the spin degrees of freedom within LSDA, the ZGNRs are predicted to have a magnetic insulating ground state with ferromagnetic ordering at each zigzag edge and antiparallel spin orientation between the two edges. The spatial spin distributions of the ground state in the case of 12-ZGNR is displayed in Fig. 4(a). The small spin-orbit coupling [28] in carbon atoms is neglected in the present study, and we label one spin orientation as $-$ -spin (red) and the opposite as $+$ -spin (blue) in Fig. 4(a). The total energy difference per edge atom between nonspin-polarized and spin-polarized edge states increases from 20 meV ($N_z = 8$) to 24 meV ($N_z = 16$). These energy differences are further stabilized by an antiferromagnetic coupling between the two edges. The total energy difference between ferromagnetic and antiferromagnetic couplings between edges, however, decreases as N_z increases and eventually becomes negligible if the width is significantly larger than the decay length of the spin polarized edge states [12]. The ferromagnetic-antiferromagnetic energy differences per unit cell are 4.0, 1.8, and 0.4 meV for the 8-, 16-, and

32-ZGNR, respectively. Our LSDA results agree with previous studies [4, 11, 12] and consistent with a theorem based on the Hubbard Hamiltonian on a bipartite lattice [29]. Though in finite range spontaneous magnetic ordering in a one dimensional Heisenberg model is ruled out [30], spin orderings in nanoscale system are realizable in practice [31, 32, 33, 34] at finite temperature assisted by the enhanced anisotropy on substrates [33, 34].

The energy gaps in ZGNRs originate from the staggered sublattice potentials resulting from the magnetic ordering, which introduce bandgaps for electrons on a honeycomb hexagonal lattice [35]. This is realized because the opposite spin states on opposite edges occupy different sublattices respectively (black rectangles on the left side and grey ones on the right belong to different sublattice respectively in Fig. 1(b)). So, the ZGNRs can be considered as the magnetic analog of a single BN sheet because the former has a bandgap which originates from the exchange potential difference on the two sublattices while the bandgap of the latter is from the ionic potential difference between boron and nitrogen atoms located on the different sublattices [36]. The Hamiltonian (H) and Bloch wavefunctions ($\psi_{nk}(\mathbf{r})$) of the ground states satisfy $[H; T] = 0$ and $T \psi_{nk} = \psi_{nk}$ where T is the time-reversal symmetry operator and M a mirror symmetry operator interchanging sites on opposite sides. Hence, $+$ and $-$ spin states are degenerate in all bands and have the same gap as shown in Fig. 4(b).

Since the strength of the staggered potentials in the middle of the ribbon decreases as the width increases, the LSDA bandgaps of ZGNRs are inversely proportional to the width. The calculated energy gaps (in eV) can be fitted by $E_g(w_z) = 9.33/(w_z + 15.0)$ with w_z in Angstroms when $N_z \geq 8$ as shown in Fig. 4(c). It is also shown that the energy splitting at $k = \pi/2$ (in Fig. 4(b)) converges to 0.53 eV (32-ZGNR) from 0.51 eV (8-ZGNR).

In summary, we have shown that graphene nanoribbons with homogeneous armchair or zigzag shaped edges all have energy gaps which decrease as the widths of the system increase [37]. The role of the edges are crucial for determining the values and scaling rule for the bandgaps.

Y.-W.S. thanks F. G. Justino, D. P. Rendergast, and C. Girit for discussions. This research was supported by NSF Grant No. DMR04-39768 and by the Director, Office of Science, Office of Basic Energy under Contract No. DE-AC02-05CH11231. Computational resources have been provided by NSF at NPACI and DOE at NERSC.

Email: syblouie@berkeley.edu

- [1] G. D resselhaus, M. S. D resselhaus, P. C. Eklund, Science of Fullerenes and Carbon Nanotubes: Their Properties and Applications (Academic Press, 1996).
 [2] L. Chico et al, Phys. Rev. Lett. 76, 971 (1996).
 [3] P. L. McEuen, M. S. Fuhrer, H. Park, IEEE Trans. Nanotechnol. 1, 78 (2002).

- [4] M. Fujita, K. Wakabayashi, K. Nakada, K. Kusakabe, J. Phys. Soc. Jpn. 65, 1920 (1996).
 [5] K. Nakada, M. Fujita, G. Dresselhaus, M. S. Dresselhaus, Phys. Rev. B 54, 17954 (1996).
 [6] K. Wakabayashi, M. Fujita, H. Ajiki, M. Sigrist, Phys. Rev. B 59, 8271 (1999).
 [7] M. Ezawa, Phys. Rev. B 73, 045432 (2006).
 [8] L. Breney and H. A. Fertig, Phys. Rev. B 73, 235411 (2006).
 [9] K.-I. Sasaki, S. Murakami, R. Saito, J. Phys. Soc. Jpn. 75, 074713 (2006).
 [10] D. A. Abanin, P. A. Lee, L. S. Levitov, Phys. Rev. Lett. 96, 176803 (2006).
 [11] S. Okada and A. Oshiyama, Phys. Rev. Lett. 87, 146803 (2001).
 [12] H. Lee et al, Phys. Rev. B 72, 174431 (2005).
 [13] Y.-W. Son, M. L. Cohen, S. G. Louie, Nature, in press (2006).
 [14] Y. Miyamoto, K. Nakada, M. Fujita, Phys. Rev. B 59, 9858 (1999).
 [15] T. Kawai, Y. Miyamoto, O. Sugino, Y. Koga, Phys. Rev. B 62, R16349 (2000).
 [16] H. Hirata, Appl. Surf. Sci. 222, 374 (2004).
 [17] K. S. Novoselov et al, Nature 438, 197 (2005).
 [18] Y. Zhang, Y.-W. Tan, H. L. Stormer, P. Kim, Nature 438, 201 (2005).
 [19] C. Berger et al, Science 312, 1191 (2006).
 [20] C. Berger et al, J. Phys. Chem. B 108, 19912 (2004).
 [21] M. L. Sadowski et al, cond-mat/0605739.
 [22] S. Reich, J. Maultzsch, C. Thomassen, P. Ordejón, Phys. Rev. B 66, 035412 (2002).
 [23] J. M. Soler et al, J. Phys. Condens. Matter 14, 2745 (2002) and references therein.
 [24] We expect that the generalized gradient approximation would not change the main results.
 [25] We have tested the various values for electronic temperature from 12 K to 580 K but found no variation of the size of the gap.
 [26] C. A. Coulson, J. Phys. Chem. 56, 311 (1952).
 [27] D. Porezag et al, Phys. Rev. B 51, 12947 (1995).
 [28] G. Dresselhaus, M. Dresselhaus, J. G. Mavroides, Carbon 4, 433 (1966).
 [29] E. H. Lieb, Phys. Rev. Lett. 62, 1201 (1989).
 [30] N. D. Mermin and H. Wagner, Phys. Rev. Lett. 17, 1133 (1966).
 [31] P. Gambardella et al, Nature 416, 301 (2002).
 [32] A. Delin, E. Tosatti, R. Weht, Phys. Rev. Lett. 92, 057201 (2004).
 [33] J. Dorantes-Dávila and G. M. Pastor, Phys. Rev. Lett. 81, 208 (1998).
 [34] P. Gambardella et al, Phys. Rev. Lett. 93, 077203 (2004).
 [35] C. L. Kane and E. J. Mele, Phys. Rev. Lett. 95, 146802 (2005).
 [36] X. Blase, A. Rubio, S. G. Louie, M. L. Cohen, Phys. Rev. B 51, 6868 (1995).
 [37] LDA Kohn-Sham gaps in general underestimate the quasiparticle band gaps of semiconductors. (See, e.g., M. S. Hybertsen and S. G. Louie, Phys. Rev. B 34, 5390 (1986)). We expect an overall increase in the value of the gap calculated here when considering quasi-particle corrections using the GW approximation as discussed in T. Miyake and S. Saito, Phys. Rev. B 68, 155424 (2003); *ibid.* 72, 073404 (2005).